Research Article

Single-cell and multi-cell performance analysis of OFDM index modulation

Shangbin Wu[1] ✉, Maziar Nekovee[1]

[1]*Samsung R&D Institute UK, Staines-upon-Thames, UK*
✉ *E-mail: shangbin.wu@samsung.com*

Abstract: This study addresses the achievable rate of single cell and sum rate of multi-cell orthogonal frequency division multiplexing (OFDM) index modulation (IM). The single-cell achievable rate of OFDM-IM with Gaussian input is calculated using a multi-ary symmetric channel. Then, the cumulative distribution function of multi-cell OFDM-IM is investigated by stochastic geometry. Furthermore, it is proved in this study that the probability density function of noise plus inter-cell interference in multi-cell OFDM-IM with quadrature-amplitude modulation follows a mixture of Gaussians (MoGs) distribution. Next, parameters of the MoG distribution are estimated using a simplified expectation maximisation algorithm. Upper bound of sum rates of multi-cell OFDM-IM is derived. Furthermore, analytic and simulated results are compared and discussed.

1 Introduction

The fifth generation (5G) cellular network is emerging to satisfy the unprecedented growth in data traffic and the number of connected devices. A key performance indicator of 5G is the ability to provide smooth quality of user experience at cell edges, which requires above 1 Gbps data rates. Recently, orthogonal frequency division multiplexing (OFDM) index modulation (IM) [1] was proposed as one of the 5G enabling technologies, as it has advantages such as increase in per subcarrier transmit power and reduction in inter-cell interference (ICI). It was reported in [2, 3] that the ICI of legacy OFDM networks follows a Gaussian distribution which caused most throughput degradation. However, the ICI of OFDM-IM is not Gaussian distributed. Therefore, OFDM-IM is able to provide room to optimise data rate at cell edges. The philosophy behind OFDM-IM is that only one of a number of OFDM subcarriers is active when transmitting symbols. In addition to the information carried by the transmitted symbol, the subcarrier index can also be used to convey information. The idea of conveying information via indexes was first proposed in the spatial domain, i.e. spatial modulation (SM) [4]. A variant version of OFDM-IM was proposed in [5], where bits were divided into blocks of bits before the OFDM-IM modulator. Basar *et al.* in [6] studied practical implementation issues of OFDM-IM such as maximum likelihood (ML) detector, log-likelihood ratio detector, and impact of channel estimation errors. A low-complexity ML detector for OFDM with in-phase/quadrature IM was discussed in [7], which was implemented with a priori knowledge of noise variance. In [8], additional interleaving was introduced to subcarriers in correlated channels, in order to provide extra diversity gain to the OFDM-IM. Later, the combination of OFDM-IM and SM was proposed in [9], where the symbol domain, subcarrier domain, and spatial domain formed a three-dimensional signal space. Then, the generalised OFDM-IM was introduced in [10], where multiple subcarriers were active. The information conveyed by the index relies on different combinations of active subcarrier indexes. When the transmitted symbols of OFDM-IM are quadrature-amplitude modulation (QAM) symbols, this type of OFDM-IM was named frequency QAM (FQAM) [2]. Studies of OFDM-IM in [1, 2, 6–9] focused on bit error rate and frame error rate performance.

Achievable rates of OFDM-IM with different settings were reported in [11–13]. OFDM-IM with finite constellation input was discussed in [11], where a closed-form lower bound of the achievable rate was derived. The applications of OFDM-IM for underwater acoustic communications as well as achievable rate with finite constellation input were investigated in [12]. Although achievable rate of OFDM-IM with Gaussian input was investigated in [13], closed-form expression was not provided in [13].

Also, the performance of OFDM-IM in multi-cell scenarios has been less studied. System level simulations (SLSs) over typical hexagonal multi-cell network are able to provide certain insights of multi-cell performance of wireless networks with OFDM-IM. However, there are two drawbacks of SLSs. First, SLSs are time consuming. Second, the hexagonal multi-cell network layout is usually not fulfilled in realistic situations, where base stations (BSs) are approximately distributed in a uniform manner. Therefore, it is beneficial to have analytic results on the performance of multi-cell scenarios. This can be investigated via a mathematics tool called stochastic geometry [14–19], where BSs were assumed to be distributed following a Poisson point process (PPP). In this case, the cumulative distribution function (CDF) of the signal-to-interference plus noise (SINR) was expressed in closed form in different scenarios such as *ad hoc* networks [16], cellular networks [18], and cooperative networks [19].

Hong *et al.* in [2] studied the statistics of ICI in multi-cell OFDM-IM with QAM inputs. The generalised Gaussian distribution was used to approximate the distribution of noise plus ICI. However, the exact distribution of noise plus ICI of multi-cell OFDM-IM with QAM inputs was missing in the literature. In this paper, this exact distribution will be found.

The contributions of this paper are listed as below:

i. The subcarrier index detection error probability of single-cell OFDM-IM with Gaussian input is conducted. Then, closed-form single-cell achievable rate of OFDM-IM with Gaussian input is derived.
ii. The CDF of SINR of multi-cell OFDM-IM is derived using stochastic geometry.
iii. The distribution of ICI of multi-cell OFDM-IM with QAM input is derived showing that it follows a mixture of Gaussians (MoGs) distribution. In addition, the parameters of the probability density function (PDF) of ICI are computed using a simplified expectation maximisation (EM) algorithm. Then, the upper bound of sum rates of multi-cell OFDM-IM with QAM input is studied.

The rest of this paper is structured as follows. Section 2 gives a general description of the system model. Achievable rate of single-cell OFDM-IM with Gaussian input will be investigated in Section
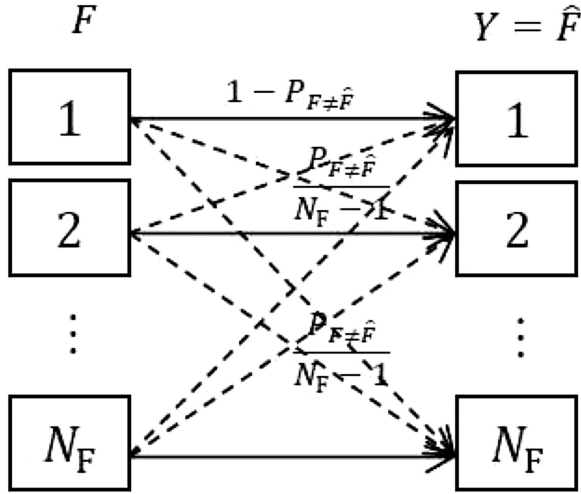
Fig. 1 *Diagram of an N_F-ary symmetric channel*

3. Section 4 will study the CDF of SINR of multi-cell OFDM-IM with stochastic geometry. Also, the distribution and its parameters of ICI are analysed. Simulation results and analysis are presented in Section 5. Conclusions are drawn in Section 6.

2 System model

Let us consider a downlink multi-cell network using OFDM-IM, where a target user equipment (UE) is located at the origin. BSs are distributed as a homogeneous PPP with density λ. The set of all BSs is denoted as $\mathcal{S}$ and the set of BSs interfering the target UE is denoted as $\mathcal{S}'$. Let α be the pathloss coefficient. Assume that the OFDM-IM system has N_F subcarriers, then $\log_2 N_F$ bits are conveyed by subcarrier indexes. N_B is the number of BSs. Let F be the subcarrier index, which is a uniformly distributed random variable defined on $\{1, 2, \ldots, N_F\}$ and let $\mathcal{H}_\xi = \{h_{\xi,1}, h_{\xi,2}, \ldots, h_{\xi,N_F}\}$ be the set of all channel coefficients from the ξth BS to the target user on these subcarriers. The channel coefficients $h_{\xi,k}$ ($1 \leqslant k \leqslant N_F$) are independently and identically distributed (i.i.d.) zero-mean unit variance complex Gaussian random variables. In practise, this i.i.d. channel assumption can be achieved by introducing interleaving between subcarriers as [8]. The interleaving can be done via a pseudo-random sequence, which is shared by the BS and UE, such that the BS and UE can map or de-map between the original subcarrier indices and the interleaved subcarrier indices. Throughout this paper, we assume that the target UE has perfect knowledge of the channel coefficients from the associated BS, but no knowledge from other BSs. Let the ξth BS be the associated BS of the target UE. The distance between the ξth BS and the target UE is d and the distance between the lth BS and the target UE is d_l ($\forall l \neq \xi$). Then, the received signal Y of the target UE can be expressed as

$$Y = \sqrt{T_\xi} H_\xi X_\xi + N + I, \tag{1}$$

where N is a zero-mean complex Gaussian noise with variance σ_N^2, H_ξ is uniformly distributed random variable defined on $\mathcal{H}_\xi$, X_ξ is the transmitted symbol from the ξth BS to the target user, T_ξ is the average received power (including transmit power, path loss, and shadow fading) from the ξth BS to the target UE, and I is the interference from other BSs. Thus, interference I can be written as

$$I = \sum_{l \neq \xi} \sqrt{T_l} H_l X_l \zeta_l, \tag{2}$$

where $\zeta_l = 1$ if the lth BS is transmitting on the same subcarrier as the ξth BS and $\zeta_l = 0$ if the lth BS is not transmitting on the same subcarrier as the ξth BS. This is due to a basic property of OFDM-

IM, which activates only one subcarrier in each transmission period.

3 Single-cell OFDM-IM

Achievable rate of OFDM-IM with QAM input and other finite constellation inputs can be found in [2, 11–13]. However, closed-form expression for achievable rate of single-cell OFDM-IM with Gaussian input is missing in the literature. Therefore, to fill this gap, single-cell achievable rate of OFDM-IM with Gaussian input is analysed in this section. Since single cell is considered, subscript ξ representing the ξth BS is dropped for brevity and the interference term I equals 0. Information of OFDM-IM is conveyed by the symbol X and the frequency index F. The achievable rate r in this paper is defined by the average maximum achievable mutual information between the information source (X, F) and the destination Y, which can be characterised as

$$
\begin{aligned}
r &= \mathrm{E}[\max\ I(X, F; Y)] \\
&\approx \mathrm{E}[\max\ I(X; Y|F)] + \mathrm{E}[\max\ I(F; Y)] \\
&= r_1 + r_2.
\end{aligned} \tag{3}
$$

Since the channel coefficient H is determined once the subcarrier index F is determined, the achievable rate of the single-cell OFDM-IM generated by the symbol in terms of signal-to-noise ratio (SNR) ρ can be calculated using the achievable rate of the Rayleigh fading channel, i.e.

$$
\begin{aligned}
r_1(\rho) &= \mathrm{E}[\max\ I(X; Y|F)] \\
&= \mathrm{E}[\max\ I(X; Y|H)] \\
&= \int_0^\infty \log_2(1 + z\rho)e^{-z}\,\mathrm{d}z \\
&= -\frac{1}{\ln 2}\mathrm{Ei}\!\left(-\frac{1}{\rho}\right)\exp\!\left(\frac{1}{\rho}\right),
\end{aligned} \tag{4}
$$

where $\mathrm{Ei}(\cdot)$ is the exponential integral [20] defined by $\mathrm{Ei}(-z) = -\int_z^\infty (e^{-t}/t)\mathrm{d}t$. The SNR ρ can easily be controlled by adjusting the BS transit power to compensate path loss and shadow fading in a single-cell scenario.

The calculation of r_2 is equivalent to determining how much information is retrieved from Y when the information is conveyed on a certain subcarrier F. The information retrieving process is not perfect because of the existence of noise. As a result, the subcarrier index maybe incorrectly detected. Let $\hat{F}$ be the detected subcarrier index and $P_{F \neq \hat{F}}$ be the subcarrier index detection error probability and denote $P_{F = k \cap \hat{F} = l}$ as the probability that the kth subcarrier is used, whereas the lth subcarrier is detected. With the assumption that the channel coefficients on subcarriers are i.i.d., it can be observed that $P_{F = f_k \cap \hat{F} = f_l} = \frac{P_{F \neq \hat{F}}}{N_F - 1}(\forall l \neq k)$. Hence, the channel between F and Y can be abstracted by an N_F-ary symmetric channel as depicted in Fig. 1. The achievable rate $r_2(\rho)$ of an N_F-ary symmetric channel depends on the subcarrier index detection error probability and can be presented as [21]

$$r_2(\rho) = \log_2 N_F - H_b\!\left[P_{F \neq \hat{F}}(\rho)\right] - P_{F \neq \hat{F}}(\rho)\log_2(N_F - 1), \tag{5}$$

where $H_b[\mu]$ is the binary entropy function defined by $H_b[\mu] = -\mu\log_2\mu - (1 - \mu)\log_2(1 - \mu)$. To calculate $r_2(\rho)$, we need to compute $P_{F \neq \hat{F}}(\rho)$ with the following lemma.

Lemma 1: The subcarrier index detection error probability can be presented as

$$P_{F \neq \hat{F}}(\rho) = 1 - \sqrt{\frac{\pi}{2}} \sum_{k=0}^{N_F-1} C_{N_F-1}^k ($$

$$-1)^{N_F-k-1} \frac{[1 - \Phi(\sqrt{((N_F-k)/2\rho(N_F-k-1)))})]}{\sqrt{\rho(N_F-k-1)(N_F-k)}} \exp \qquad (6)$$

$$\left(\frac{N_F-k}{2\rho(N_F-k-1)} \right),$$

where $C_{N_F-1}^k$ is the binomial coefficient defined by $C_{N_F-1}^k = (((N_F-1)!)/k!(N_F-k-1))$ and $\Phi(z)$ is the error function defined by $\Phi(z) = (2/\sqrt{\pi}) \int_0^z e^{-t^2} \, dt$.

Proof: Conditioning on X, errors occur in the detection of the subcarrier index when the received signal power on the intended subcarrier is less than any one of the rest subcarriers. Owing to the symmetry, it is sufficient to calculate the subcarrier index detection error probability assuming that the first subcarrier is used. Let Y_k ($1 \leqslant k \leqslant N_F$) be the received signal on the kth subcarrier. Then, $Y_1 = HX + N$ and $Y_2, Y_3, \ldots, Y_{N_F}$ have the same distribution as N. With the condition $X = x$, $|Y_1|^2$ is an exponential random variable with mean $x^2 + \sigma_N^2$ and $|Y_{k \neq 1}|^2$ are exponential random variables with mean σ_N^2. Let $G_{|Y_2|^2}$ be the CDF of $|Y_2|^2$. Then, $P_{F \neq \hat{F}|X=x}(\rho)$ is calculated as (see (7)) Since x follows a Gaussian distribution with zero mean and variance one, the PDF of x^2 is the Gamma distribution with degree of freedom one, i.e. $p_{X^2}(z) = (1/\sqrt{2\pi z})e^{-(z/2)}$. Unconditioning the frequency index detection error probability, $P_{F \neq \hat{F}}(\rho)$ can be obtained as

$$P_{F \neq \hat{F}}(\rho) = \int_{-\infty}^{\infty} P_{F \neq \hat{F}|X=x}(\rho) p_X(x) \, dx$$

$$= \int_0^{\infty} P_{F \neq \hat{F}|X=z}(\rho) p_{X^2}(z) \, dz$$

$$= 1 - \sum_{k=0}^{N_F-1} \int_0^{\infty} \frac{C_{N_F-1}^k (-1)^{N_F-k-1}}{z\rho(N_F-k-1)+N_F-k} \frac{1}{\sqrt{2\pi z}} e^{-z/2} \, dz. \qquad (8)$$

Solving the integral [20], (6) can be obtained. □

4 Multi-cell OFDM-IM

After deriving the single-cell sum rate of OFDM-IM with Gaussian inputs in Section 3, multi-cell OFDM-IM is investigated in this section. In practical system, finite alphabet inputs are usually used instead of Gaussian inputs. Moreover, the impact of ICI needs to be studied. Therefore, OFDM-IM with QAM inputs is assumed in this section and other types of constellations can be obtained in a similar manner. The CDF of SINR, the PDF of noise plus ICI, and the multi-cell sum rate will be derived.

4.1 CDF of SINR

Since only one subcarrier of the target UE and the associated BS is active, the density of interfering BSs to the target UE is one N_Fth of the original BS density. Let $\tilde{\rho}$ denote the SINR and P_T denote the transmit power of each BS. The derivation of the CDF of SINR is directly generalised from [16]. The normalised interference power $\mathcal{I}$ from other BSs transmitting on the same subcarrier to the target user can be computed as

$$\mathcal{I} = \sum_{l \in \mathcal{S}'} |h_l|^2 |d_l|^{-\alpha}. \qquad (9)$$

The channel h_ξ between the target user and his associated BS follows Rayleigh distribution. Hence, $|h_\xi|^2$ is an exponentially distributed random variable. The CDF $G_{\tilde{\rho}}(\tilde{\rho})$ of SINR can then be computed as [16]

$$G_{\tilde{\rho}}(\tilde{\rho}) = 1 - \Pr\left\{ \frac{P_T |h_\xi|^2 d^{-\alpha}}{\sigma_N^2 + P_T \mathcal{I}} \geqslant \tilde{\rho} \right\}$$

$$= 1 - \exp(-P_T^{-1} d^\alpha \tilde{\rho} \sigma_N^2) E[\exp(-d^\alpha \tilde{\rho} \mathcal{I})]. \qquad (10)$$

Using the Laplace transform of the exponential function and the probability generating functional [16], the expectation part in (10) can be expressed as

$$E[\exp(-d^\alpha \tilde{\rho} \mathcal{I})] = E[\exp(-z\mathcal{I})]_{|z=d^\alpha \tilde{\rho}}$$

$$= \exp\left(-\frac{\lambda}{N_F} \int_{\mathfrak{R}^2} \frac{1}{1+z^{-1}|y|^\alpha} \, dx \right)_{|z=d^\alpha \rho}$$

$$= \exp\left(-\frac{\lambda}{N_F} z^{2/\alpha} \frac{2\pi^2}{\alpha \sin(2\pi/\alpha)} \right)_{|z=d^\alpha \tilde{\rho}}. \qquad (11)$$

Hence, the CDF $G_{\tilde{\rho}}(\tilde{\rho})$ of multi-cell OFDM-IM can be expressed as

$$G_{\tilde{\rho}}(\tilde{\rho}) = 1 - \exp(-P_T^{-1} d^\alpha \tilde{\rho} \sigma_N^2) \exp\left(-\frac{\lambda}{N_F} d^2 \tilde{\rho}^{(2/\alpha)} \frac{2\pi^2}{\alpha \sin(2\pi/\alpha)} \right). \qquad (12)$$

To avoid 0 at the denominator in (12), α should be larger than 2. Typical values of α are between 2 and 4.

4.2 PDF of noise plus interference

The exact PDF of noise plus ICI of multi-cell OFDM-IM with QAM inputs remained unanswered in the literature. Generalised

$$P_{F \neq \hat{F}|X=x}(\rho) = \Pr\left\{ |Y_1|^2 < \max\left\{ |Y_2|^2, \ldots, |Y_{N_F}|^2 \right\} | X = x \right\}$$

$$= 1 - \int_0^{\infty} p_{|Y_1|^2}(z) G_{|Y_2|^2}^{N_F-1}(z) \, dz$$

$$= 1 - \int_0^{\infty} \frac{\exp\{-(z/(x^2+\sigma_N^2))\}}{x^2+\sigma_N^2} \sum_{k=0}^{N_F-1} \binom{N_F-1}{k} (-1)^{N_F-k-1} e^{-(1/\sigma_N^2)(N_F-k-1)z} \, dz$$

$$= 1 - \sum_{k=0}^{N_F-1} \binom{N_F-1}{k} (-1)^{N_F-k-1} \int_0^{\infty} \frac{\exp\{-(z/(x^2+\sigma_N^2)) - (z/\sigma_N^2)(N_F-k-1)\}}{x^2+\sigma_N^2} \, dz \qquad (7)$$

$$= 1 - \sum_{k=0}^{N_F-1} \binom{N_F-1}{k} (-1)^{N_F-k-1} \frac{1}{(x^2/\sigma_N^2)(N_F-k-1)+N_F-k}$$

$$= 1 - \sum_{k=0}^{N_F-1} C_{N_F-1}^k (-1)^{N_F-k-1} \frac{1}{x^2\rho(N_F-k-1)+N_F-k}.$$

1: Initialize Ω and $\mathbf{v}$ randomly

2: E step: Compute

$$\eta_{ak} = \frac{\omega_k \mathcal{CN}(\tau_a; 0, \sigma_k^2)}{\sum_{k=1}^{Q} \omega_k \mathcal{CN}(\tau_a; 0, \sigma_k^2)} \tag{18}$$

3: M step: Update $\sigma_k^{2,\mathrm{new}}$ and ω_k^{new} according to

$$\sigma_k^{2,\mathrm{new}} = \frac{1}{\sum_{a=1}^{N_s} \eta_{ak}} \sum_{a=1}^{N_s} \eta_{ak} |\tau_a|^2 \tag{19}$$

$$\omega_k^{\mathrm{new}} = \frac{\sum_{a=1}^{N_s} \eta_{ak}}{N_s}. \tag{20}$$

4: Repeat E step and M step until convergence condition is met.

Fig. 2 *EM algorithm for parameter estimation of noise plus ICI in OFDM-IM systems*

Gaussian distributions were used to approximate the PDF in [2, 3]. In this section, the exact PDF of noise plus ICI will be derived showing that noise plus ICI is MoG distributed. Let $Q = 2^{N_B - 1}$ and denote ψ as the noise plus ICI, i.e. $\psi = N + \sum_{l \neq \xi} \sqrt{T_l} H_l X_l \zeta_l$.

Theorem 2: The PDF p_ψ of noise plus ICI in multi-cell OFDM-IM with QAM inputs follows an MoG distribution, i.e.:

$$p_\psi(z) = \sum_{k=1}^{Q} \omega_k \mathcal{N}(z; 0, \sigma_k^2). \tag{13}$$

Proof: In this proof, 4QAM is used for simplicity. The distribution of one ICI term, i.e. $\psi_l = h_l X_l \zeta_l$, is first computed. It can be easily shown that $h_l X_l \sim \mathcal{CN}(0, 1)$. Also, the PDF of ζ_l for 4QAM can be expressed as $p_{\zeta_l}(\zeta_l) = (1/N_F)\delta(\zeta_l - 1) + ((N_F - 1)/N_F)\delta(\zeta_l)$ which is directly obtained from the fact that the subcarrier index is chosen uniformly. Next, according to the product distribution

$$\begin{aligned} p_{h_l X_l \zeta_l}(z) &= \int_{-\infty}^{\infty} p_{\zeta_l}(\tau) \frac{1}{\pi} \exp(-|z/\tau|^2) \frac{1}{|\tau|} \, d\tau \\ &= \frac{1}{N_F} \frac{1}{\pi} \exp(-|z|^2) + \frac{N_F - 1}{N_F} \lim_{\epsilon \to 0} \frac{1}{\pi\epsilon} \exp\left(-\frac{|z|^2}{\epsilon}\right) \quad (14) \\ &= \frac{1}{N_F} \frac{1}{\pi} \exp(-|z|^2) + \frac{N_F - 1}{N_F} \delta(z). \end{aligned}$$

Hence, the PDF of one interference term is a weighted sum of a Gaussian function and a Dirac delta function. Using the properties of convolution, the PDF of the total interference can be expressed as (see (15)) where $*$ denotes the convolution operator and $\tilde{\omega}_k \geqslant 0$ with $\sum_k \tilde{\omega}_k = 1$. By adding the noise term, the PDF p_ψ of noise plus ICI can be calculated as

$$\begin{aligned} p_\psi(z) &= \mathcal{CN}(z; 0, \sigma_N^2) * \left[\sum_{k=1}^{Q-1} \tilde{\omega}_k \mathcal{CN}(z; 0, \tilde{\sigma}_k^2) + \tilde{\omega}_Q \delta(z) \right] \\ &= \sum_{k=1}^{2^{N_B - 1}} \omega_k \mathcal{CN}(z; 0, \sigma_k^2), \end{aligned} \tag{16}$$

where $\omega_k \geqslant 0$ with $\sum_k \omega_k = 1$. $\square$

Lemma 3: The PDF p_Y of the received signal Y in multi-cell OFDM-IM with QAM inputs follows an MoG distribution, i.e.:

$$p_Y(y) = \sum_{k=1}^{Q} \omega_k' \mathcal{CN}(y; 0, \sigma_k'^2). \tag{17}$$

Proof: This can be obtained directly from Theorem 2 and (1), because the desired signal also follows a Gaussian distribution. $\square$

Next, parameters $\boldsymbol{\Omega} = \begin{bmatrix} \omega_1 & \omega_2 \cdots \omega_Q \end{bmatrix}$ and $\mathbf{v} = \begin{bmatrix} \sigma_1^2 & \sigma_2^2 \cdots \sigma_Q^2 \end{bmatrix}$ need to be estimated. It is well known that the EM algorithm has been widely used to estimate parameters of MoG distributions. Detailed derivations of EM algorithm for MoG parameter estimation are beyond the scope of this paper. Interested readers can find details in [22]. In particular, for FQAM, the traditional EM algorithm [22] can be further simplified because the means of the channel, the transmitted symbol, the ICI, and noise are all zero. The simplified EM algorithm is presented in Fig. 2. Assuming samples of the noise plus ICI are measured as $\{\tau_a\}_{a=1}^{N_s}$. First, Ω and $\mathbf{v}$ are randomly chosen as initialisation. Second, E step and M step are operated iteratively until a certain convergence condition is met. The number of Gaussian functions in (16) grows exponentially with the number of BSs, which is impractical due to high complexity. However, only a small number of BSs are dominating the total interference. In this case, a small number Q' ($Q' \ll Q$) of Gaussian functions will be sufficient to approximate the distribution of noise plus ICI. The parameters of the PDF p_Y of the received signal, i.e. $\boldsymbol{\Omega}' = \begin{bmatrix} \omega_1' & \omega_2' \cdots \omega_{Q'}' \end{bmatrix}$ and $\mathbf{v} = \begin{bmatrix} \sigma_1'^2 & \sigma_2'^2 \cdots \sigma_{Q'}'^2 \end{bmatrix}$, can also be estimated via the same procedure.
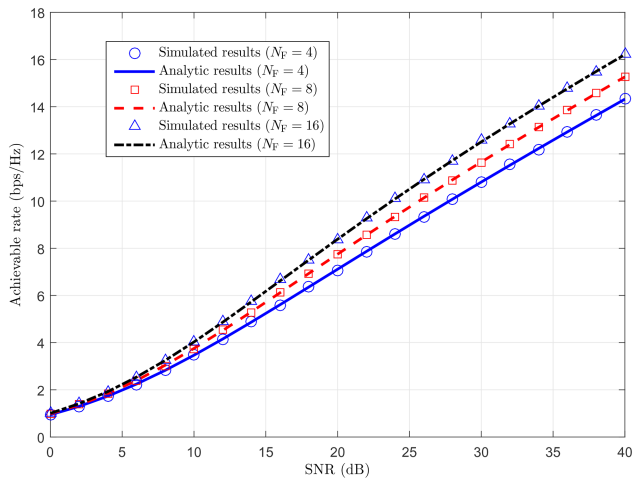
4.3 Multi-cell sum rate

The multi-cell sum rate r_3 of OFDM-IM is defined by the mutual information between the received signal and the information source as

$$\begin{aligned} r_3 &= \mathrm{E}[\max I(X, F; Y)] \\ &= \mathrm{E}[H(Y)] - \mathrm{E}[H(Y|X, F)] \\ &= H(Y) - H(Y|X, F), \end{aligned} \tag{21}$$

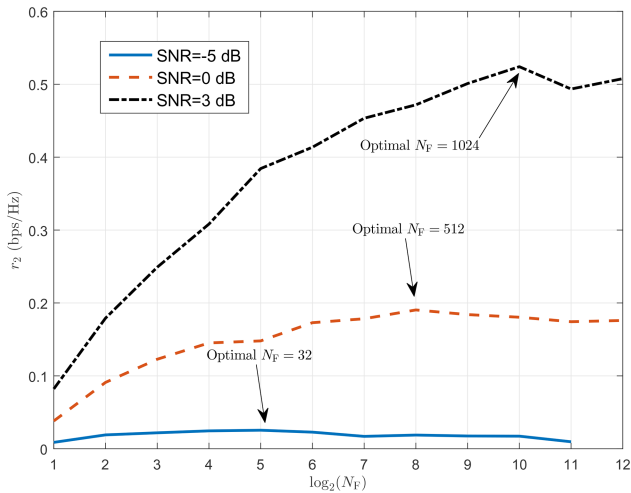$$p_{h_1 X_1 \zeta_1}(z) * \cdots * p_{h_{\xi-1} X_{\xi-1} \zeta_{\xi-1}}(z) * p_{h_{\xi+1} X_{\xi+1} \zeta_{\xi+1}}(z) * \cdots * p_{h_{N_B} X_{N_B} \zeta_{N_B}}(z)$$

$$= \sum_{k=1}^{Q-1} \tilde{\omega}_k \mathcal{CN}(z; 0, \tilde{\sigma}_k^2) + \tilde{\omega}_Q \delta(z), \tag{15}$$
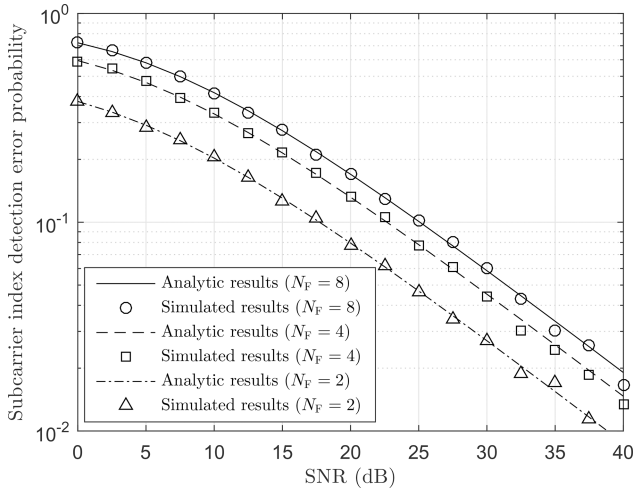
Fig. 3 *Subcarrier index detection error probability of single-cell OFDM-IM*

Fig. 4 *Achievable rates of single-cell OFDM-IM with different numbers of subcarriers*

Fig. 5 *Achievable rates contributed by different numbers of subcarriers and the optimal N_F*

where $H()$ is the entropy function. The maximum operator in (21) is removed because of the QAM symbol and the expectation operator are removed because the entropies of Y and $N+I$ are already expectation values. Although closed-form integral of (21) is not feasible because of the summation inside the logarithm function, upper bounds of the sum rate can be evaluated.

Since the entropy function $H()$ is concave, using Jensen's inequality, $H(Y|X, F)$ is lower bounded by

$$H(Y|X, F) = H\left(\sum_{k=1}^{Q} \omega_k \mathcal{CN}(z; 0, \sigma_k^2)\right) \geqslant \sum_{k=1}^{Q} \omega_k H\left(\mathcal{CN}(z; 0, \sigma_k^2)\right)$$

$$= \frac{1}{2} + \sum_{k=1}^{Q} \omega_k \log_2(2\pi e \sigma_k).$$

(22)

On the contrary, $H(Y)$ is upper bounded by [23] (see (23)) To sum up, the multi-cell sum rate of OFDM-IM r_3 is upper bounded by

$$r_3 \leqslant \sum_{k'=1}^{Q} \omega_{k'}' \log_2\left(\frac{2\pi e \sigma_{k'}'}{\omega_{k'}'}\right) - \sum_{k=1}^{Q} \omega_k \log_2(2\pi e \sigma_k).$$

(24)

This upper bound provides insights in sum rate performance of multi-cell OFDM-IM.

5 Results and analysis

Subcarrier index detection error probability and achievable rates of single-cell OFDM-IM with different number of subcarriers are depicted in Figs. 3 and 4, respectively. In both figures, analytic results match simulated results well. It can be observed in Fig. 4 that when the SNR is relatively low, the achievable rate contributed by subcarrier indexes is not significant. However, when SNR increases gradually, the gaps between achievable rates with different numbers of subcarriers first increase and then become stable.

Fig. 5 shows single-cell OFDM-IM achievable rate contributed by subcarrier indexes with different numbers of subcarriers and different SNR values. From (5), r_2 tends to zero when N_F tends to infinity. This suggests that the benefit of increasing N_F is diminishing and there is an optimal number of N_F such that r_2 reaches its peak. Closed-from expression of the optimal value of N_F is not available. However, this can be calculated by numerical results. It is shown in Fig. 5 that the optimal value of N_F increases with the SNR.

In multi-cell SLSs, thermal noise with power density -173 dBm/Hz [24] is assumed in the multi-cell network. Also, the bandwidth of each subcarrier is 15 kHz [24]. In this case, the noise power per subcarrier can be calculated by $\sigma_N^2 = 7.5 \times 10^{-11}$ W.

Fig. 6 illustrates the CDFs of SINR in terms of different values of N_F in the multi-cell OFDM-IM scenario. The SINR is larger when N_F is larger, because the target UE has a smaller probability of being interfered, where ICI is more spread in the frequency domain. In addition, the simulated results reasonably well align with analytic results.

The PDF of the real part of noise plus ICI of multi-cell OFDM-IM with 4QAM inputs is illustrated in Fig. 7. The total number of BSs is 19 and the inter-site distance is 100 m. It can be observed that the MoG distribution derived in this paper fits simulation excellently. The generalised Gaussian model proposed in [2, 3] and the Gaussian model are also shown in Fig. 7. However, these two models fail to match the realistic noise plus ICI well. The
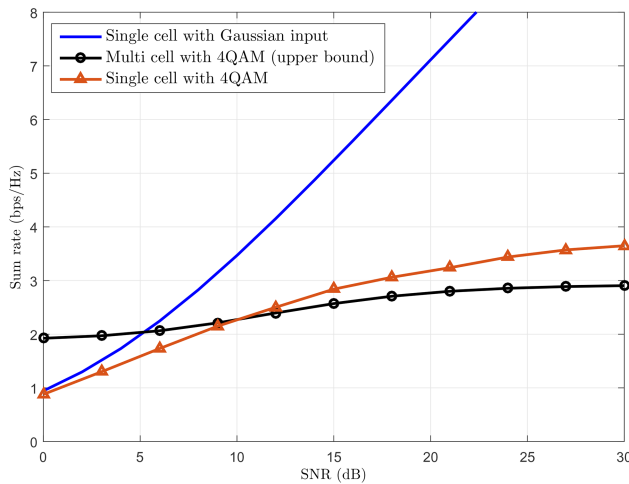
$$H(Y) = H\left(\sum_{k=1}^{Q} \omega_k' \mathcal{CN}(y; 0, \sigma_k'^2)\right) \leqslant -\int \sum_{k=1}^{Q} \omega_k' \mathcal{CN}(y; 0, \sigma_k'^2) \log_2\left(\omega_k' \mathcal{CN}(y; 0, \sigma_k'^2)\right) \mathrm{d}y$$

(23)

$$= \frac{1}{2} + \sum_{k=1}^{Q} \omega_k' \log_2(2\pi e \sigma_k' / \omega_k').$$
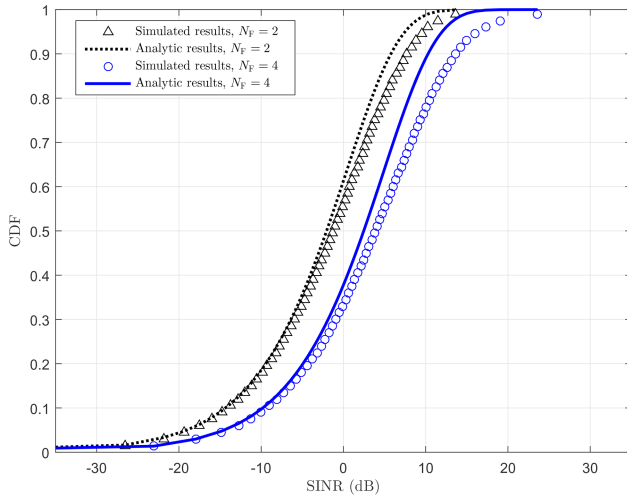
Fig. 6 *Comparison of CDFs of SINR with respect to different numbers of subcarriers of multi-cell OFDM-IM ($\lambda = 10^{-4}$, $\alpha = 3$, $P_T = 40$W, and $d = 50$ m)*
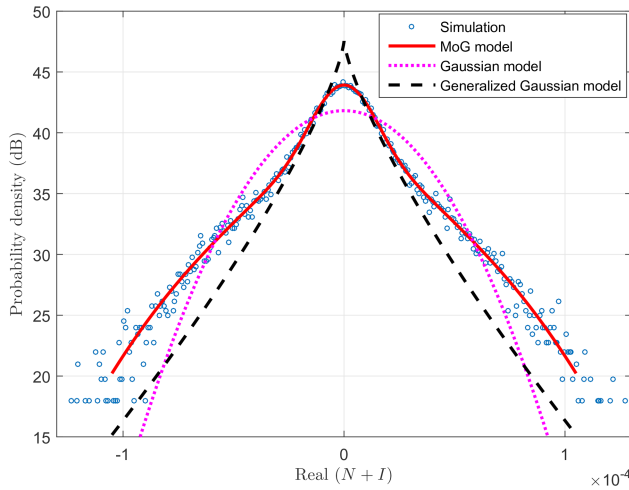
Fig. 7 *PDF of the real part of noise plus ICI of multi-cell OFDM-IM with 4QAM inputs ($N_B = 19$, $\alpha = 3$, $P_T = 40$ W, $d = 50$ m, and $Q' = 4$)*

Fig. 8 *Upper bound of sum rates of multi-cell OFDM-IM ($N_B = 19$ and $N_F = 4$)*

generalised Gaussian model is able to capture the peak while it does not model the spread well. On the other hand, the Gaussian model has better alignment with the PDF spread than the generalised Gaussian model, but it is not accurate to model the peak.

The upper bound of sum rates of multi-cell OFDM-IM with 4QAM is depicted in Fig. 8. Single-cell achievable rates with Gaussian input and 4QAM are included as reference. It can be observed that the sum rate of multi-cell OFDM-IM is at least ∼20% worst than single-cell results because of ICI. When the SNR is smaller, though the multi-cell result outperforms the other two single-cell results, this is caused by the upper limit.

6 Conclusions

In this paper, single-cell achievable rate and multi-cell statistical properties of SINR, ICI, and sum rate for OFDM-IM have been studied. It has been shown that the increase of the number of subcarriers does not improve the single-cell achievable rate in the low SNR regime. The main benefit of more subcarriers appears in multi-cell scenarios, where less BSs will be interfering the target UE. In addition, the PDF of noise plus ICI has been derived for OFDM-IM with QAM input, showing that noise plus ICI follows an MoG distribution. The parameters of the MoG distribution have been estimated by a simplified EM algorithm in this paper. Later, upper bound of sum rate of multi-cell OFDM-IM has been derived, which can be used as performance guideline for OFDM-IM networks. For future work, it will be practical to use the PDF of noise plus ICI to develop multi-cell OFDM-IM signal detection algorithms. Also, the analysis method in this paper can be extended to N_F-ary asymmetric channel to investigate achievable rates of generalised OFDM-IMs.

7 Acknowledgment

8 References

[1] Abu-adhiga, R., Haas, H.: 'Subcarrier-index modulation OFDM'. Proc. PIMRC'09, Tokyo, Japan, September 2009, pp. 177–181
[2] Hong, S., Sagong, M., Lim, C., *et al.*: 'Frequency and quadrature-amplitude modulation for downlink cellular OFDMA networks', *IEEE J. Sel. Areas Commun.*, 2014, **32**, (6), pp. 1256–1267
[3] Seol, C., Cheun, K.: 'A statistical inter-cell interference model for downlink cellular OFDMA networks under log-normal shadowing and multipath Rayleigh fading', *IEEE Trans. Commun.*, 2009, **57**, (10), pp. 3069–3077
[4] Mesleh, R.Y., Haas, H., Sinanovic, S., *et al.*: 'Spatial modulation', *IEEE Trans. Veh. Technol.*, 2008, **57**, (4), pp. 2228–2241
[5] Tsonev, D., Sinanovic, S., Haas, H.: 'Enhanced subcarrier index modulation (SIM) OFDM'. Proc. Globecom'11, Huston, USA, December 2011, pp. 1–5
[6] Basar, E., Aygolu, U., Panayirci, E., *et al.*: 'Orthogonal frequency division multiplexing with index modulation', *IEEE Trans. Signal Process.*, 2013, **61**, (22), pp. 5536–5549
[7] Zheng, B., Chen, F., Wen, M., *et al.*: 'Low-complexity ML detector and performance analysis for OFDM with in-phase/quadrature index modulation', *IEEE Commun. Lett.*, 2015, **19**, (11), pp. 1893–1896
[8] Xiao, Y., Wang, S., Dan, L., *et al.*: 'OFDM with interleaved subcarrier-index modulation', *IEEE Commun. Lett.*, 2014, **18**, (8), pp. 1447–1450
[9] Datta, T., Eshwaraiah, H.S., Chockalingam, A.: 'Generalized space and frequency index modulation', *IEEE Trans. Veh. Technol.*, 2016, **65**, (7), pp. 4911–4924
[10] Fan, R., Yu, Y.J., Guan, Y.L.: 'Generalization of orthogonal frequency division multiplexing with index modulation', *IEEE Trans. Wireless. Commun.*, 2015, **14**, (10), pp. 5350–5359
[11] Wen, M., Cheng, X., Ma, M.: 'On the achievable rate of OFDM with index modulation', *IEEE Trans. Signal Process.*, 2015, **64**, (8), pp. 1919–1932
[12] Wen, M., Cheng, X., Yang, L., *et al.*: 'Index modulated OFDM for underwater acoustic communications', *IEEE Commun. Mag.*, 2016, **54**, (5), pp. 132–137
[13] Ishikawa, N., Sugiura, S., Hanzo, L.: 'Subcarrier-index modulation aided OFDM - will it work?', *IEEE Access*, 2016, **4**, pp. 2580–2593
[14] Baccelli, F., Blaszczyszyn, B.: 'Stochastic geometry and wireless networks volume I: theory.', *Found. Trends Netw.*, 2010, **3**, (3–4), pp. 249–449
[15] Baccelli, F., Blaszczyszyn, B.: 'Stochastic geometry and wireless networks volume II: applications.', *Found. Trends Netw.*, 2010, **4**, (1–2), pp. 1–312
[16] Baccelli, F., Blaszczyszyn, B., Muhlethaler, P.: 'An Aloha protocol for multihop mobile wireless networks', *IEEE Trans. Inf. Theory*, 2006, **52**, (2), pp. 421–436
[17] ElSawy, H., Hossain, E., Haenggi, M.: 'Stochastic geometry for modeling, analysis, and design of multi-tier and cognitive cellular wireless networks: a survey', *IEEE Commun. Surv. Tutor.*, 2013, **15**, (3), pp. 996–1019, third quarter

[18]   Andrews, J.G., Baccelli, F., Ganti, R.K.: 'A tractable approach to coverage and rate in cellular networks', *IEEE Trans. Commun.*, 2011, **59**, (11), pp. 3122–3134

[19]   Baccelli, F., Giovanidis, A.: 'A stochastic geometry framework for analyzing pairwise-cooperative cellular networks', *IEEE Trans. Wireless. Commun.*, 2015, **14**, (2), pp. 794–808

[20]   Gradshteyn, I.S., Ryzhik, I.M.: '*Table of integrals, series, and products*' (Academic Press, Burlington, 2007, 7th edn.)

[21]   Weidmann, C., Lechner, G.: 'A fresh look at coding for *q*-ary symmetric channels', *IEEE Trans. Inf. Theory*, 2012, **58**, (11), pp. 6959–6967

[22]   Bishop, C.M.: '*Pattern recognition and machine learning*' (Springer, New York, 2007)

[23]   Huber, M.F., Bailey, T., Durrant-Whyte, H.*, et al.*: 'On entropy approximation for Gaussian mixture random variables'. Proc. MFI'08, Seoul, Korea, August 2008, pp. 181–188

[24]   3GPP T. R. 36.814: 'Further advancements for E-UTRA physical layer aspects.', V1.7.0, February 2010